THE JOURNAL OF
PHYSICAL CHEMISTRY
LETTERS
A JOURNAL OF THE AMERICAN CHEMICAL SOCIETY

pubs.acs.org/JPCL Letter

Two-Dimensional MXene Flakes with Large Second Harmonic Generation and Unique Surface Responses

Shaun M. Debow, Haley Fisher, Jesse B. Brown, Mallory Liebes, Hui Wang, T. T. Trinh Phan, T. Kien Mac, M. Tuan Trinh,* Yanqing Su, Zachary Zander, Mark S. Mirotznik, Robert L. Opila, and Yi Rao*

Cite This: *J. Phys. Chem. Lett.* 2024, 15, 11087−11096 Read Online

ACCESS | Metrics & More | Article Recommendations | Supporting Information

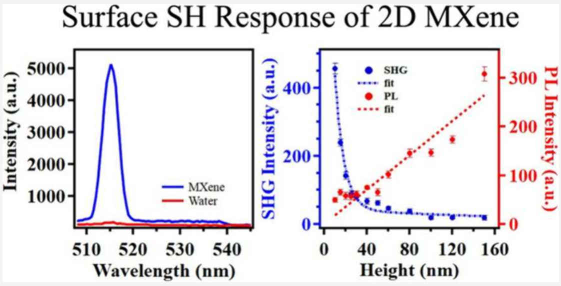

ABSTRACT: MXenes are a family of two-dimensional (2D) materials with broad and varied applications in biology, materials science, photonics, and environmental remediation owing to their layered structure and high surface area-to-volume ratio. MXenes have exhibited significant nonlinear optical characteristics, which have been primarily explored in the context of photonics applications, yet the second-harmonic generation (SHG) behavior of MXenes remains an unexplored aspect of their optical properties. Herein, we demonstrate and quantify large second-order responses of 2D $Ti_3C_2T_x$ MXenes both in aqueous solutions and on a silicon substrate for the first time. MXene flakes showed strong second-harmonic scattering (SHS) in a dilute suspension with a sensitivity of less than 0.1 μg/mL. Angle-dependent SHS experiments further found that the second-order responses originate from coherent 2D dipole radiation. Through confocal and atomic force microscopies, we found that the intense SHG signal from free-standing MXene flakes increases exponentially with decreasing thickness, while two-photon fluorescence increases linearly with thickness. The second-order susceptibility of the MXenes was determined to be 3.6 pm V^{-1} with a thickness of 10 nm, almost twice of that for an often-used SHG crystal, beta barium borate. We further explored surface properties of the MXene sheets by investigating the SHS responses upon addition of organic dye molecules to the system. It was found that the adsorption of crystal violet (CV) obeys a Langmuir adsorption model while the addition of malachite green (MG) resulted in almost no change in SHG intensity, even though the adsorption capacities for both CV (61.3 ± 1.7 mg/g) and MG (54.8 ± 2.8 mg/g) are similar. Such a stark difference in adsorption characteristics between cationic organic CV and MG dyes is likely due to their distinct orientational orderings on the MXene surfaces. This work opens many possibilities for the further employment of the family of 2D materials in photonics, optics, and surface catalysis applications.

MXenes are a family of 2D materials consisting of transition metal carbides and nitrides taking the form $M_{n+1}X_nT_x$, where M is an early transition metal, X is C or N, and T are surface terminal groups on M sites including OH, O, F, and Cl.[1] Since their fabrication from MAX (Ti_3AlC_2) in 2011 by Naguib et al.,[2] MXenes have been a major topic of research in materials science and chemistry.[1,3,4] This is due to the utility of MXenes in photocatalysis,[5−9] energy storage,[10−13] biosensing,[14] electrochemistry,[15−18] and water treatment for environmental remediation.[19−22] For example, MXenes have been used in H_2 production[23,24] and CO_2 reduction,[25,26] as well as methane[27] and methanol[28] production by photocatalytic reactions. MXenes also have been utilized in electrochemical hydrogen evolution[29] and water oxidation[30] showing significant catalytic promise. The unique layered structure of MXenes has also been exploited as a means for the removal of metal ions in solution,[31−33] desalination,[34,35] and even treatment of organic contaminants including antibiotics[36] and dyes.[37,38] Hybrid MXene-gold nanoparticle composites have even provided enhanced sensitivity for biosensing applications for viral mutations.[14] These unique structure and properties of MXenes materials stem from their 2D layered structure which provides excellent surface area for functionalization and adsorbate interactions. Such adsorption can lead to areas of broken symmetry, where nonlinear spectroscopic methods are uniquely sensitive to detecting these areas by measuring the second-order nonlinear response. However, until now, the intrinsic second-order nonlinear optical properties and molecular adsorption on MXenes remain unexplored.

Received: September 9, 2024
Revised: October 9, 2024
Accepted: October 24, 2024
Published: October 29, 2024

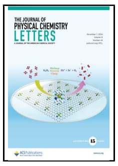

https://doi.org/10.1021/acs.jpclett.4c02646
J. Phys. Chem. Lett. 2024, 15, 11087−11096

Second harmonic generation (SHG) is a second order nonlinear optical process which is very sensitive to the crystal symmetry of materials. This technique has been used extensively over the past decade to investigate the optical and physiochemical properties of other 2D materials, including crystal symmetry, stacking alinement, crystal strain tension, phase transition, magnetism, among many others.[39,40] In some of the first demonstrations of SHG with 2D materials, it was shown that the breaking inversion symmetry of MoS_2, which forbade bulk SHG character, enhanced the nonlinear response of atomically thin and odd-numbered layered 2D sheets.[41,42] Further investigation by Li et al. developed a relationship between the crystalline and electronic structures of 2D MoS_2 whereby interlayer electronic coupling occurred and therefore electronic structure changed as a function of layer thickness.[43] Second-harmonic character has been exhibited in other 2D semiconductor materials such as WSe_2[44] and InSe.[45] More recent examples of this material-instrument combination and response include observations of strain-induced changes in SHG light patterns from 2D graphene, GaSe, WS_2, In_2Se_3,[46] penta-CdO_2 sheets,[47] and designer self-intercalated tantalum sulfide sheets with spontaneous and scalable second-harmonic character.[48] Interestingly, SHG has recently been used as a tool to investigate the effects of mechanical forces applied on MXene flakes, as well as their piezoelectric properties. For example, it was shown that mechanical strain affected the linear and nonlinear optical properties of Sc_2CT_2 MXenes with significant anisotropicity.[49] Furthermore, changes is in the SH character of monolayer Ti_3C_2 MXene sheets was used to identify crystal orientations for further monolayer piezoelectric applications.[50] While the SHG has been used for sensing of MXene properties, the SH character of MXenes has not yet been thoroughly quantified.

MXenes have seen applications in optics and nonlinear optics as well.[51] For example, Ti_3CN showed promise as a saturable absorption material for mode-locking femtosecond lasers, where it was employed in a near-IR laser with subpicosecond pulse durations at a high repetition rate.[52] Furthermore, the nonlinear character of another MXene, $Ti_3C_2T_x$, was examined demonstrating a large nonlinear absorption coefficient and a negative nonlinear refractive index on par with that of graphene.[53] $Ti_3C_2T_x$ also showed great potential in near-IR mode locking applications, obtaining a pulse duration of hundreds of femtoseconds. Hybrid $Ti_3C_2(OH)_2/Ti_3C_2F$ MXenes have also found utility in nonlinear optical experiments as a saturable absorber in the near-IR and was deployed in a Q-switching application.[54] Later, the nonlinear character of $Ti_3C_2T_x$, was systematically studied where its nonlinear absorption coefficients, negative nonlinear refractive indices, and third-order susceptibilities were quantified.[55] Further study of $Ti_3C_2T_x$, using ultrafast transient absorption has shown that the material exhibits a long bleaching recovery time which contributes to its usefulness in broadband Q-switching applications.[56] Other investigations have shown that $Ti_3C_2T_x$ can undergo a laser-induced structural change from flat to rippled in hundreds of fs, with ripples that were aligned with the incident laser polarization.[57] By comparing surface terminations and their effect on MXene optical properties, it was shown that = O rich surfaces resulted in saturable absorption but −OH rich termination resulted in reverse saturable absorption, and the nonlinear absorption coefficient of the −OH rich sample was over 50% greater than that of the pristine sample.[58] Although the nonlinear optical characteristics of MXenes have been investigated and produced interesting photonic properties, nonlinear methods have not been used with MXenes to probe chemical processes *in situ*.

Unlike 2D transition metal dichalcogenides such as MoS_2, MXenes, specifically $Ti_3C_2T_x$, have exhibited metallic electronic character, where its conductivity decreased upon photoexcitation.[59] Accordingly, MXenes may be expected to exhibit SHG character similar to other metals such as gold and silver,[60,61] but this has not yet been demonstrated. Additionally, MXene surfaces have shown excellent potential for functionalization to extend their applicability. In one such case, phenylsulfonic-functionalized MXenes exhibited a 2-fold increase in capacitance and excellent stability for better electrochemical energy storage applications.[62] In another example, $Ti_3C_2T_x$ was functionalized with aminosilane groups which resulted in a pH-tunable surface charge and extended their utility.[63] MXene 2D sheets have also been used as a photothermal ablation tool for tumors where their functionality can assist in interfacing in biological systems.[64] In a recent study, boro-organic functionalized $Ti_3C_2T_x$ showed excellent fire and smoke retardant characteristics in a composite material for industrial applications.[65] The extensive applicability of MXenes in many applications, stemming from their diverse surface functionalization and coupled with their distinctive physiochemical attributes, highlights their significance and emphasizes the need to enhance our understanding of these materials.

While the use of MXenes to remediate organic pollution in aqueous systems is not novel, the complete exploration and optimization of this approach have not been achieved, thus creating opportunity for further investigation. Building upon their adsorptive capabilities, recent studies have also investigated the potential of MXenes to adsorb and degrade organic dyes in aqueous media.[37,38] An early demonstration of the ability of $Ti_3C_2T_x$ to adsorb organics was with methylene blue (MB), which followed a Freundlich isotherm over a Langmuir isotherm, and demonstrated the affinity of MXenes for cationic adsorbates resulting in a strong and irreversible binding.[37] Later, it was shown that alkalized $Ti_3C_2T_x$ resulted in increased interlayer spacing that increased its adsorption capacity for MB[38] as well as Congo red.[66] MXene also has shown an impressive adsorption capacity for MB and methyl orange.[67] While the adsorption of organic dyes by MXenes has been studied repetitiously, these works focus on the adsorption capacity of the dye, instead of *in situ* monitoring adsorption mechanism of dyes onto MXenes. Given the unique metallic traits of MXenes which can contribute to their nonlinear optical properties, along with their unique surface chemistry which hosts functionalization and adsorption unlike other 2D semiconductors, we believe that this combination of characteristics may make MXenes ideal for investigating using SHG methods to detect contaminant adsorption and uptake.

In this work, we demonstrate, to the best of our knowledge, the first report of both SHG detection of MXenes in aqueous solutions and quantitative evaluation of second-order nonlinear optical properties of few layer $Ti_3C_2T_x$ MXenes. Using second-harmonic and atomic force microscopies, we found that the SHG intensity strongly depends on the sample thickness: the thicker sample, the smaller SHG signal; possibly becoming canceled out by dipole symmetry for multilayer samples. We then quantify the second-order susceptibility of $Ti_3C_2T_x$ MXenes, a metric by which materials' nonlinear optical properties can be assessed. To better understand the

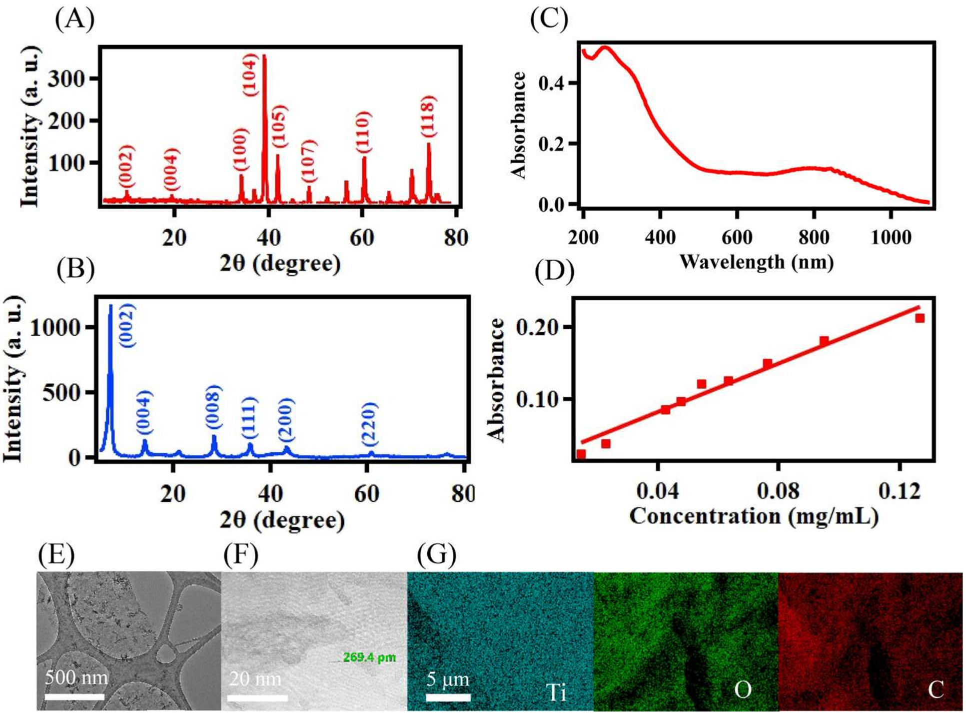

Figure 1. XRD pattern of MAX phase (A) and $Ti_3C_2T_x$ MXenes (B). (C) UV−vis absorption spectrum of an aqueous MXene suspension. (D) UV−vis calibration curve of different MXene concentrations. (E, F) TEM images with scale bars of 500 and 20 nm, respectively. G) EDS elemental mapping of (left to right) Ti, O, and C with a scale bar of 5 μm.

surface/interface properties of the $Ti_3C_2T_x$ MXene flakes, we then investigated their dye adsorption capabilities using crystal violet (CV) and malachite green (MG) in aqueous suspensions by monitoring their adsorption *in situ* using second-harmonic scattering (SHS) spectroscopy. This work highlights the impressive SH character of MXenes and uses it to obtain ppb sensitivities for dye contaminants in addition to other applications in nonlinear optics and photonics.

■ EXPERIMENTAL SECTION

Second Harmonic Scattering (SHS) Experiments. Light was sourced from a femtosecond laser amplifier system (Carbide, Light Conversion), operating at a repetition rate of 100 kHz and an output power of 5.0 W. As schematically depicted in Figure S1, the laser pulse was centered at 1030 nm with a duration of 170 fs. The polarization of the 1030 nm pulse was adjustable via a half-wave plate, while a thin-film polarizer was employed to select the polarization of the SHS signal. A lens with a focal length of 5.0 cm was utilized for the 1030 nm light, resulting in focal spot diameters of approximately 35 μm. The pulse energy before the sample was 0.8 μJ. A spectrometer (Acton 300i, Princeton Instruments) combined with a charge-coupled device (CCD) detector (Princeton Instruments, LN/CCD-1340/400) was used for spectral collection.

Forward-collected SHS experiments were conducted with the sample in a 10 mm quartz cuvette while angle-dependent scattering experiments used an NMR tube with a 5 mm outside diameter and 0.5 mm wall thickness. The collection arm of the instrument was mounted on a rotating stage (PR50CC: Newport) which focused the collected signal into an optical fiber (FC-UVIR600−1-BX 1904207: AVANTES), and a LabView program was used to correlate scattering angles with the collected spectra. A 3° angular resolution was obtained by using a 2 mm slit. Angle-dependent scattering spectra were collected from −75° to 75° at 2° increments. Polarizations of the incident and collected light are defined as H-polarized being within the scattering plane (horizontal plane), and V-polarized being perpendicular to the scattering plane, resulting in four polarization combinations of HH, HV, VH, and VV, in order of incident light followed by the SH signal.

AFM and SHG Imaging. Atomic force microscopy (AFM) measurements were conducted using a silicon tip in contact mode, combined with a confocal microscope (NTEGRA Spectra II, NT-MDT Inc.). For SHG imaging measurements, the sample was excited by femtosecond laser pulses at a wavelength of 900 nm with a pulse duration of <100 fs and a repetition rate of 80 MHz (Mai Tai, Spectra Physics). The objective used was 100x with NA = 0.7 and a long working distance (Mitutoyo). SHG images were acquired by scanning the laser beam using a Galvo mirror and detecting the SHG and photoluminescence signals with an EM-CCD camera. All measurements were performed under ambient conditions. The samples for AFM and SHG imaging measurements were prepared by drop-casting a dilute solution of MXenes onto a silicon substrate.

$Ti_3C_2T_x$ MXene Preparation. Multilayer $Ti_3C_2T_x$ MXene flakes were prepared by etching Ti_3AlC_2 MAX phase 500 mesh powder.[68] 1.0 g of the MAX powder was slowly added to 30 mL of 12 M HCl and 3 M HF, then stirred for 20 h at 45 °C with a condenser column to minimize product loss. After etching, the sample was washed repeatedly with deionized (DI) water (18.2 MΩ cm) until the supernatant reached a pH of 5. To delaminate the sample, 25 mL of 1.0 M LiCl was added to the neutralized MXene with about 25 mL of water used to transfer the sample.[69] The mixture was stirred and heated at 65 °C for 1 h under argon, followed by 3 washes with

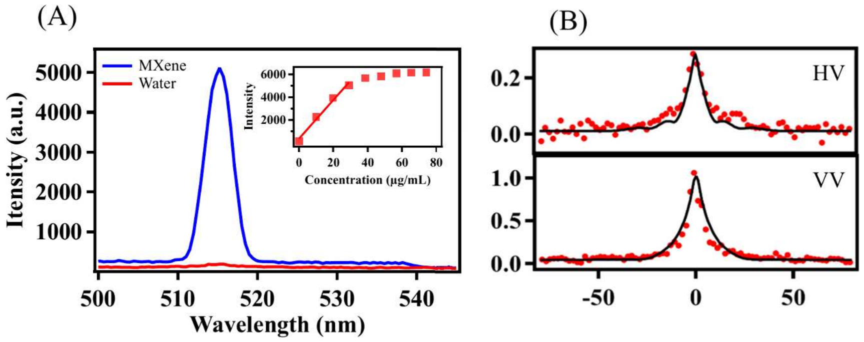

Figure 2. (A) Emission spectra of 0.06 mg/mL $Ti_3C_2T_x$ MXenes in DI water (blue) and DI water (red) at HH polarization under 1030 nm excitation. The inset shows SHG intensity of the MXenes suspended in DI water from 0 to 80 μg/mL. (B) Angle-dependent SHS under HV (red dots, top) and VV (red dots, bottom) polarization combinations from the suspension of 60 μg/mL $Ti_3C_2T_x$ MXene flakes normalized with angle-dependent VV-polarized hyper-Rayleigh scattering (HRS) from water. Black curves represent the fitted data using the Rayleigh-Gan-Debye scattering model.

DI water. The prepared MXenes were stored suspended in argon-purged DI water.

Chemicals. MAX phase powders were purchased from Laizhou Kai Kai Ceramic Materials Company Ltd. HCl (certified ACS plus) was purchased from Fisher Chemical and HF (was purchased from Sigma-Aldrich. LiCl (99%) was purchased from Sigma-Aldrich. Argon gas was purchased from Airgas. Malachite green was purchased from Acros Organics and crystal violet was purchased from Alfa. All components were rinsed extensively with methanol (HPLC-UV grade, Pharmco) and 18.2 MΩ cm ultrapure water.

RESULTS AND DISCUSSION

The quality of our as-prepared $Ti_3C_2T_x$ MXenes from MAX phase was characterized by X-ray diffraction (XRD), ultraviolet−visible (UV−vis) spectroscopy, and transmission electron microscopy (TEM). As shown in Figure 1(A), the diffraction peaks obtained for the pristine MAX phase powder were in accordance with JCPDS no. 52−0875. These peaks at 9.78°, 19.72°, 34.06°, 39.04°, 41.84°, 48.46°, 60.28°, and 74.08° were assigned to (002), (004), (100), (104), (105), (107), (110), and (118) crystal planes, respectively. The XRD pattern in Figure 1(B) for MXene also correlated with JCPDS no. 32−1383, with the peaks at 6.96°, 13.86°, 28.3°, 35.66°, 43.28°, and 60.68° being assigned to (002), (004), (008), (111), (200), and (220) crystal planes, respectively. After etching the MAX phase, the most prominent peak in the MAX phase XRD pattern at 39.04° disappeared indicating complete etching of the Al layers.[2] In addition, the Ti_3C_2 peaks at 9.78° and 19.72° broadened and were negatively shifted to 6.96° and 13.86°, respectively, further signaling the Al layers were etched and the interlayer distance increased. UV−vis spectroscopy was used to characterize the MXene and to determine the concentration for the prepared samples. In Figure 1(C), a representative UV−vis spectrum of a suspension of 0.02 mg/mL MXenes in DI water results in a broad peak around 770 nm with additional peaks at shorter wavelengths consistent with the literature.[70,71] The absorption peak at 770 nm was used to construct the calibration curve shown in Figure 1(D), which exhibits a linear fit at concentrations up to 0.1 mg/mL; beyond which significant light scattering was observed and affected linearity. TEM was used to investigate the morphology of the as-prepared MXenes revealing several hundred nanometer diameter flakes, as shown in Figure 1(E). Furthermore, high-resolution TEM (HRTEM) in Figure 1(F) shows that the interlayer spacing was 0.26 nm, which matches previous reports.[72] Figure 1(G) verifies the elimination of Al from the prepared MXenes with TEM elemental mapping depicting the spatial distributions of Ti, C, and O with a ratio of 56.9%, 21.2%, and 14.2%, respectively.[73,74] Overall, these structural and morphological analyses indicate the complete etching of MXenes from MAX phase powder and demonstrated a high-quality product.

To probe the second-order nonlinear optical properties of MXenes, we first implement second-harmonic scattering (SHS) spectroscopy of the $Ti_3C_2T_x$ flakes suspended in DI water. Figure 2(A) shows emission spectra at 2ω for samples containing DI water (red) and 0.06 mg/mL MXene suspended in DI water (blue) under an input fundamental light of ca. 1030 nm. SHG is a second-order nonlinear optical process in which two degenerate photons are coincident on a sample and are annihilated to produce a new photon whose frequency is twice the incident frequency: 515 nm. Here we can see a large signal, over 60 times more intense from the MXene suspension than that from the water sample. Under the dipole approximation, SHG is forbidden from systems possessing inversion symmetry and is therefore forbidden from bulk media. This large SH response from the MXene indicates that such symmetry is broken at the water/MXene interface. Additionally, the coherent SHS response from MXenes suspensions should increase linearly with concentration of the scatterer.[75−77] Along these lines, different concentrations of MXene SHS in DI water were collected and their peak intensities at 515 nm were plotted as a function of concentration in the inset of Figure 2(A). A linear increase was observed for concentrations up to 0.03 mg/mL, after which the intensity stabilizes, possibly due to excessive scattering form sample turbidity. The sensitivity of SHS signal from MXene flakes of less than 0.1 μg/mL is readily achieved and is only limited to the hyper-Rayleigh scattering (HRS) signal from water. These results demonstrate a very intense SHS response from MXenes in a suspension which is coherent in nature.

To better understand the origin of the SHS intensity, angle-dependent scattering experiments were carried out for the 0.06 mg/mL $Ti_3C_2T_x$ MXene samples in DI water under HV and VV polarization combinations. These angle-dependent intensities, normalized with the HRS response of pure water at VV polarization are shown in Figure 2(B). This figure illustrates that VV polarization configuration produces a peak

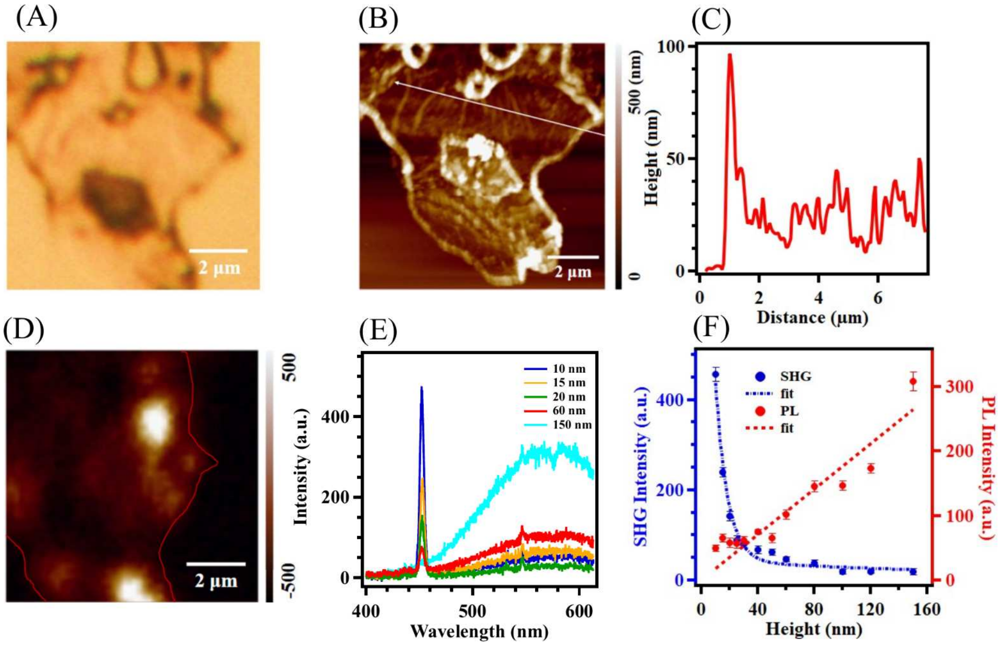

Figure 3. (A) Optical image of free-standing $Ti_3C_2T_x$ MXene flakes on a silicon substrate at 100× magnification. (B) AFM height image of the same MXene flakes. (C) AFM cross-section height profile of the sample indicated by the white line in (B). (D) SHG image of the MXene sample under 900 nm fs laser excitation; red line indicates the sample boundary. (E) Emission spectra for representative sample thicknesses under 900 nm excitation. (F) SHG and two-photon fluorescence (TPF) signals as a function of MXene thickness.

four times stronger than HV, with both having peak intensities in the forward scattering direction, 0°. HV polarization also results in satellite peak around 10°. Assuming 2D flakes of MXene with an approximate lateral size of 3 μm, as determined by optical measurements in the next section, we were able to obtain an excellent fit to the scattering patterns using Rayleigh-Gan-Debye scattering theory,[78,79] as described in the Supporting Information (SI). These experimental results further confirm that the MXenes exhibit large and coherent second-harmonic 2D dipole radiation. Although we have found that the $Ti_3C_2T_x$ MXene flakes produce large SHS responses, it is also useful to investigate the material's SH character unencumbered by the suspension medium.

To quantify the second-order susceptibility of our $Ti_3C_2T_x$ MXene flakes, thickness-dependent SHG experiments were carried out, complemented by optical and atomic force microscopies. The sample was drop-cast onto a silicon substrate, and its optical image is shown in Figure 3(A), where darker spots in the image correspond to thicker regions of the sample. The correlating AFM image is shown in Figure 3(B), with brighter regions being thicker than the darker zones. A slice of the height profile from the AFM image is shown in Figure 3(C) (taken from the white diagonal line in 3(B)), with a sample thickness ranging from about 10 to 100 nm. Using the confocal optical/AFM setup, we then collected an SHG image of the same flake, shown in Figure 3(D), where the bright spots indicate a more intense signal at 2ω. The emission spectra from the $Ti_3C_2T_x$ MXene flake at different thicknesses is shown in Figure 3(E). The thinner spectral location results in a sharp, intense SHG peak near 450 nm (incident 900 nm). In contrast, the thicker sections shown a weaker SHG peak accompanied by a broad feature centered near 580 nm, attributed to two-photon fluorescence (TPF). The intensities of these two peaks were then compared as a function of sample thickness, as shown in Figure 3(F), to better understand their origin. Here we see that while the SHG intensity decreases exponentially with increasing flake thickness, the TPF feature increases linearly with sample thickness. This relationship is indicative of cancellation of the SHG intensity by the buildup of inversion-symmetrical layers with increased MXene thickness. On the other hand, the TPF signal increases with sample thickness due to the incoherent nature of electron−hole recombination. These thickness-dependent SHG results may provide valuable insight into interlayer coupling and electronic structure., as found in other 2D materials.[41,43]

The second-order susceptibility, $\chi_i^{(2)}$ (pm V^{-1}), is a material property that quantifies the magnitude of the second-order nonlinear response. To measure the second order susceptibility of MXene flakes, we used left-handed z-cut quartz with a known second order susceptibility as a reference. As shown in the SI, the SHG intensity is directly proportional to the square of effective second-order susceptibility, $\chi_{i,eff}^{(2)}$ (pm^2 V^{-1}), which is a product of $\chi_i^{(2)}$, local field factors, and the coherence length, l_c (m) of the generated signal. The coherence length accounts for the penetration depth of the associated pulses, and the sample thickness is used when it is thinner than l_c.[80] A standard left-handed z-cut quartz crystal was used as a reference material, it has a known second-order susceptibility of 0.8 pm V^{-1} and a coherence length of 24.6 nm.[80] By comparing the SHG intensity of the unknown sample to that of the reference material (Figure S2), we were able to calculate the effective second-order susceptibility of the sample. As shown in the SI, we determined the coherent length of the $Ti_3C_2T_x$ MXene to be 13 nm,[81] resulting in $\chi_{MXene}^{(2)} = 3.6$ pm V^{-1}, which is almost twice that of the often-used SHG crystal, beta barium borate (BBO) of 1.93 pm/V.[82] The large susceptibility for $Ti_3C_2T_x$ is likely due to strong bond polarizability of the MXene structure. This hypothesis is corroborated by our AFM and SHG imaging results, where thicker sheets of $Ti_3C_2T_x$ MXenes resulted in a rapid decrease

https://doi.org/10.1021/acs.jpclett.4c02646
J. Phys. Chem. Lett. 2024, 15, 11087−11096

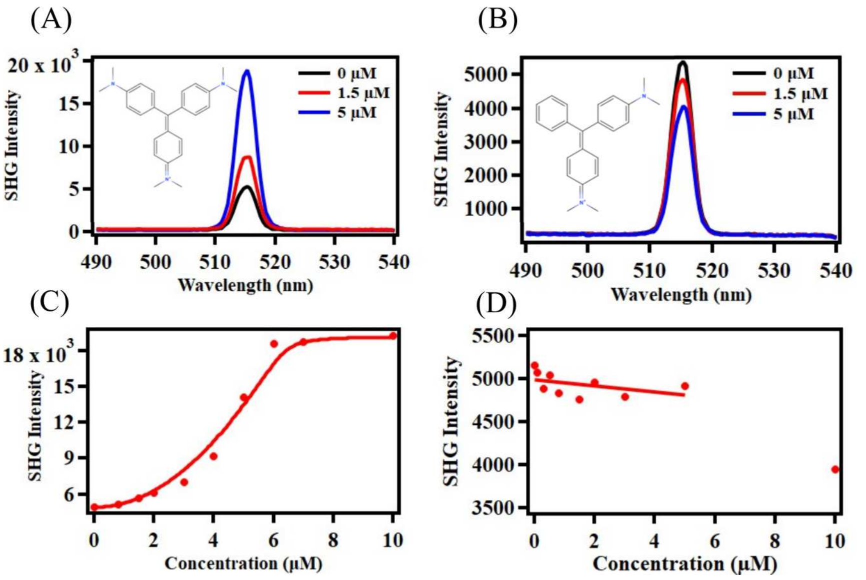

Figure 4. (A) SHG spectra of 0.06 mg/mL $Ti_3C_2T_x$ MXenes with the addition of 1.5 μM and 5.0 μM CV in DI water. (B) SHG spectra of 0.06 mg/mL MXenes with the addition of 1.5 μM and 5.0 μM MG. (C) Concentration isotherm of CV adsorbing onto the MXene suspension. (D) Concentration isotherm of MG adsorbing onto the MXene suspension. Dots represent experimental values and solid lines are to guide the eye.

in SH intensity, where misalignments of the multilayer flakes cause the 2ω intensity to be partially canceled out. An even larger second-order susceptibility is anticipated for thinner MXene materials and may differ for other moieties. Our discovery of large SHG character in MXene suggest that they could have even broader applications in various photonic devices, such as lasers and frequency conversion systems, using less expensive components through optimized packaging of the 2D flakes. Further research in this direction is needed to determine the effects of sheet orientation, surface functionalization, packing density, and different compositions to give the most efficient photonic composites.

We utilized the strong SHG character of $Ti_3C_2T_x$ MXene sheets to investigate their surface properties *in situ*, leveraging their unique structures and surfaces. Distinct from traditional 2D materials, MXenes exhibit a rich surface functionalization, featuring terminating functional groups, such as −OH, = O, -F, and -Cl, which terminate the crystal structure to form the sheets and prevent restacking. As an example, we compared the surface adsorption behaviors of crystal violet (CV) and malachite green (MG) onto MXene flakes, as shown in Figure 4. As noted above, MXenes suspended in water gives a large SHS response. As presented in Figure 4(A), the addition of CV results in a significant increase in the signal at 2ω, with an over 4-fold enhancement observed at a CV concentration of 5.0 μM. Conversely, the addition of MG to the aqueous MXene suspension leads to a slight decrease in SHS intensity, as shown in Figure 4(B). A comparison of the insets in Figures 4(A) and (B) reveals that cationic CV and MG have similar structures, with the primary difference being the absence of a -$N(CH_3)_2$ group on one phenyl of MG. This simple change results in a complete destruction of molecular symmetry, where CV has C_{3v} symmetry while, MG is reduced to D_{2d} symmetry. Since both dyes have a (+1) charge and their main difference is in symmetry, we conclude that their difference in adsorption properties is not electrostatic but is more directly the result of the MXene surface/interlayer structure. To further investigate the adsorption properties of CV and MG onto $Ti_3C_2T_x$ MXenes, we obtained concentration isotherms, as shown in Figures 4(C) and 4(D), respectively. For CV, the isotherm follows a modified Langmuir-type trend.[83−85] On the other hand, we see a slight decrease in intensity upon MG addition that does not necessarily follow any trend. Since the CV isotherm data fit well to the Langmuir model, we were able to determine the adsorption constant, K, to be $4.0(\pm 0.4) \times 10^9$ and thereby determine the adsorption free energy of CV on $Ti_3C_2T_x$ MXenes to be -12.98 ± 0.06 kcal/mol, as detailed in the SI. The adsorption free energy of CV onto the MXene surfaces is surprisingly large, and is comparable to that of MG onto a sulfate terminated, anionic functionalized MXene surface.[86] Interestingly, although MG did not result in an increase of SHS response for suspended $Ti_3C_2T_x$ MXene flakes, adsorption still occurred. As shown in the SI and Figure S3, the UV−vis absorption of both CV and MG decreased in the presence of MXene, indicating adsorption. We found that our $Ti_3C_2T_x$ MXene sheets had dye adsorption capacities of 61.3 ± 1.7 mg/g for CV and 54.8 ± 2.8 mg/g for MG. By these experiments, SHS may not always be sensitive to dye adsorption onto MXenes, possibly owing to the material's specific interfacial orientation properties.

These results demonstrate that the unique surface properties of MXenes can dramatically impact their adsorption properties by demonstrating affinity for the adsorption of both MG and CV, molecules that are chemically similar but symmetrically very different. While CV resulted in a drastic increase in the SHS intensity form the MXene suspension, but MG caused a slight decrease. Since SH methods are sensitive to orientational ordering centrosymmetry, this indicates that CV and MG adsorb to MXenes flakes with different orientational distributions. The increase in SH intensity upon adsorption of CV indicates an ordered adsorption process with aligned dipoles to promote SHG. Transversely, the reduction in SH intensity indicates a disordered adsorption process where a more random distribution of dipoles results in the SHG being canceled out. These findings are important because they indicate that for these two dyes, molecular symmetry is more impactful on MXene adsorption than electrostatics, likely a result of the surface structure of the MXenes sheets which can be altered by interacting with the dyes. The surface properties of MXenes introduces unique features into the adsorption process which calls for further mechanistic investigation. Additionally, functionalization of the MXenes sheets may be of further usefulness in linear and nonlinear optical applications, where surface structures affect the nonlinear optical properties of the material and allow it to be tailored to specific uses. We believe that SH spectroscopy can be a useful tool in studying the effects of step-by-step MXenes surface functionalization where new information about the structure–function relationships can be uncovered.

In this work, we have demonstrated large second-order nonlinear optical responses of 2D $Ti_3C_2T_x$ MXene flakes both in water solutions and on a silicon substrate and quantified its second-order nonlinear susceptibility for the first time. In an aqueous suspension, MXene flakes show strong second-harmonic scattering (SHS) in a dilute solution of less than 10 μg/mL. Angle-dependent SHS experiments further found that the second-order responses originate from coherent 2D dipole radiation. Through second-harmonic and atomic force microscopy, we found that the intense SHG signal from MXene flakes on a silicon substrate increases exponentially with decreasing thickness, while two-photon fluorescence increases linearly with sample thickness. We further explored surface properties of the MXene sheets in water solution by studying the SHS responses upon addition of organic dye molecules to the system. It was found that the adsorption of crystal violet (CV) obeys a Langmuir adsorption model while the addition of malachite green (MG) resulted in little change in SHS intensity, even though both dyes were adsorbed onto the material. Such a stark difference in adsorption characteristics between cationic organic CV and MG dyes is likely a result of the layered structure of the $Ti_3C_2T_x$ MXene sheets which appears to be sensitive to adsorbate structural symmetry. This work not only reports the first direct observation of SHG from MXenes, but also demonstrates that atomically thin MXene sheets have the largest SHG response, opening possibilities for their use in photonics and optics applications, such as lasers and frequency conversion systems. Lastly, it was shown that the combination of MXenes with SHS also may be a useful tool for detecting and adsorbing organic pollutants.

■ ASSOCIATED CONTENT

Supporting Information

The Supporting Information is available free of charge at https://pubs.acs.org/doi/10.1021/acs.jpclett.4c02646.

> Second harmonic scattering experimental details, basic principles second-harmonic scattering, calculation of second-order susceptibility for MXene flakes, determination of adsorption capacity of organic dyes onto MXene (PDF)
>
> Transparent Peer Review report available (PDF)

■ AUTHOR INFORMATION

Corresponding Authors

M. Tuan Trinh − *Department of Chemistry and Biochemistry, Utah State University, Logan, Utah 84322, United States*; Email: t.trinh@usu.edu

Yi Rao − *Department of Chemistry and Biochemistry, Utah State University, Logan, Utah 84322, United States*; orcid.org/0000-0001-9882-1314; Email: yi.rao@usu.edu

Authors

Shaun M. Debow − *U.S. Army Combat Capabilities Development Command Chemical Biological Center, Research & Technology Directorate, Aberdeen Proving Ground, Maryland 21010, United States*

Haley Fisher − *Department of Chemistry and Biochemistry, Utah State University, Logan, Utah 84322, United States*

Jesse B. Brown − *Department of Chemistry and Biochemistry, Utah State University, Logan, Utah 84322, United States*

Mallory Liebes − *Department of Chemistry and Biochemistry, Utah State University, Logan, Utah 84322, United States*

Hui Wang − *Department of Chemistry and Biochemistry, Utah State University, Logan, Utah 84322, United States*

T. T. Trinh Phan − *Department of Chemistry and Biochemistry, Utah State University, Logan, Utah 84322, United States*

T. Kien Mac − *Department of Chemistry and Biochemistry, Utah State University, Logan, Utah 84322, United States*

Yanqing Su − *Department of Mechanical and Aerospace Engineering, Utah State University, Logan, Utah 84322, United States*; orcid.org/0000-0003-0790-5905

Zachary Zander − *U.S. Army Combat Capabilities Development Command Chemical Biological Center, Research & Technology Directorate, Aberdeen Proving Ground, Maryland 21010, United States*; orcid.org/0000-0002-7801-4678

Mark S. Mirotznik − *Department of Electrical and Computer Engineering, University of Delaware, Newark, Delaware 19711, United States*

Robert L. Opila − *Department of Materials Science and Engineering, University of Delaware, Newark, Delaware 19711, United States*

Complete contact information is available at: https://pubs.acs.org/10.1021/acs.jpclett.4c02646

Author Contributions

S.M.D., H.F., J.B.B., and M.L. contributed equally to this work.

Notes

The authors declare no competing financial interest.

■ ACKNOWLEDGMENTS

Y.R. acknowledges the financial support of Reactive Chemical Systems Programs, U.S. Army Research Office (W911NF18020112). Funding was provided by the U.S. Army via the Surface Science Initiative Program (PE 0601102A Project VR9) at the U.S. Army, Combat Capabilities Development Command, Chemical Biological Center. The authors acknowledge and thank the professionals at the W. M. Keck Center for Advanced Microscopy and Microanalysis at the University of Delaware for use of their instrumentation and support. This work is also supported by the National Science Foundation under Grant No.[2045084].

■ REFERENCES

(1) Gogotsi, Y.; Anasori, B. The Rise of MXenes. *ACS Nano* **2019**, *13* (8), 8491−8494.

(2) Naguib, M.; Kurtoglu, M.; Presser, V.; Lu, J.; Niu, J.; Heon, M.; Hultman, L.; Gogotsi, Y.; Barsoum, M. W. Two-Dimensional Nanocrystals Produced by Exfoliation of Ti3AlC2. *Adv. Mater.* **2011**, *23* (37), 4248−4253.

(3) VahidMohammadi, A.; Rosen, J.; Gogotsi, Y. The world of two-dimensional carbides and nitrides (MXenes). *Science* **2021**, *372* (6547), No. eabf1581.

(4) Gogotsi, Y. The Future of MXenes. *Chem. Mater.* **2023**, *35* (21), 8767−8770.

(5) Ran, J.; Gao, G.; Li, F.-T.; Ma, T.-Y.; Du, A.; Qiao, S.-Z. Ti3C2MXene co-catalyst on metal sulfide photo-absorbers for enhanced visible-light photocatalytic hydrogen production. *Nat. Commun.* **2017**, *8* (1), 13907.

(6) Kuang, P.; Low, J.; Cheng, B.; Yu, J.; Fan, J. MXene-based photocatalysts. *Journal of Materials Science & Technology* **2020**, *56*, 18−44.

(7) Yang, J.; Wang, R.; Sun, X.; Li, Y.; Liu, J.; Kuang, X. Au/Ti3C2/g-C3N4 Ternary Composites Boost H2 Evolution Efficiently with Remarkable Long-Term Stability by Synergistic Strategies. *ACS Appl. Mater. Interfaces* **2024**, *16* (10), 12385−12397.

(8) Murali, G.; Reddy Modigunta, J. K.; Park, Y. H.; Lee, J.-H.; Rawal, J.; Lee, S.-Y.; In, I.; Park, S.-J. A Review on MXene Synthesis, Stability, and Photocatalytic Applications. *ACS Nano* **2022**, *16* (9), 13370−13429.

(9) Zhang, Q.; Li, L.; Jiang, B.; Zhang, H.; He, N.; Yang, S.; Tang, D.; Song, Y. Flexible and Mildew-Resistant Wood-Derived Aerogel for Stable and Efficient Solar Desalination. *ACS Appl. Mater. Interfaces* **2020**, *12* (25), 28179−28187.

(10) Jiang, Q.; Lei, Y.; Liang, H.; Xi, K.; Xia, C.; Alshareef, H. N. Review of MXene electrochemical microsupercapacitors. *Energy Storage Materials* **2020**, *27*, 78−95.

(11) Yin, L.; Kang, H.; Ma, H.; Wang, J.; Liu, Y.; Xie, Z.; Wang, Y.; Fan, Z. Sunshine foaming of compact Ti3C2Tx MXene film for highly efficient electromagnetic interference shielding and energy storage. *Carbon* **2021**, *182*, 124−133.

(12) Li, X.; Huang, Z.; Shuck, C. E.; Liang, G.; Gogotsi, Y.; Zhi, C. MXene chemistry, electrochemistry and energy storage applications. *Nature Reviews Chemistry* **2022**, *6* (6), 389−404.

(13) Pandey, M.; Deshmukh, K.; Raman, A.; Asok, A.; Appukuttan, S.; Suman, G. R. Prospects of MXene and graphene for energy storage and conversion. *Renewable and Sustainable Energy Reviews* **2024**, *189*, No. 114030.

(14) Chen, Z.; Wu, C.; Yuan, Y.; Xie, Z.; Li, T.; Huang, H.; Li, S.; Deng, J.; Lin, H.; Shi, Z.; Li, C.; Hao, Y.; Tang, Y.; You, Y.; Al-Hartomy, O. A.; Wageh, S.; Al-Sehemi, A. G.; Lu, R.; Zhang, L.; Lin, X.; He, Y.; Zhao, G.; Li, D.; Zhang, H. CRISPR-Cas13a-powered electrochemical biosensor for the detection of the L452R mutation in clinical samples of SARS-CoV-2 variants. *J. Nanobiotechnol.* **2023**, *21* (1), 141.

(15) Wu, X.; Ma, P.; Sun, Y.; Du, F.; Song, D.; Xu, G. Application of MXene in Electrochemical Sensors: A Review. *Electroanalysis* **2021**, *33* (8), 1827−1851.

(16) Shuai, T.-Y.; Zhan, Q.-N.; Xu, H.-M.; Huang, C.-J.; Zhang, Z.-J.; Li, G.-R. Recent advances in the synthesis and electrocatalytic application of MXene materials. *Chem. Commun.* **2023**, *59* (27), 3968−3999.

(17) Tang, Y.; Dong, L.; Wu, H. B.; Yu, X.-Y. Tungstate-modulated Ni/Ni(OH)2 interface for efficient hydrogen evolution reaction in neutral media. *Journal of Materials Chemistry A* **2021**, *9* (3), 1456−1462.

(18) Johnson, L. R.; Sridhar, S.; Zhang, L.; Fredrickson, K. D.; Raman, A. S.; Jang, J.; Leach, C.; Padmanabhan, A.; Price, C. C.; Frey, N. C.; Raizada, A.; Rajaraman, V.; Saiprasad, S. A.; Tang, X.; Vojvodic, A. MXene Materials for the Electrochemical Nitrogen Reduction—Functionalized or Not? *ACS Catal.* **2020**, *10* (1), 253−264.

(19) Zhan, X.; Si, C.; Zhou, J.; Sun, Z. MXene and MXene-based composites: synthesis, properties and environment-related applications. *Nanoscale Horizons* **2020**, *5* (2), 235−258.

(20) Kumar, J. A.; Prakash, P.; Krithiga, T.; Amarnath, D. J.; Premkumar, J.; Rajamohan, N.; Vasseghian, Y.; Saravanan, P.; Rajasimman, M. Methods of synthesis, characteristics, and environmental applications of MXene: A comprehensive review. *Chemosphere* **2022**, *286*, No. 131607.

(21) Verma, R.; Sharma, A.; Dutta, V.; Chauhan, A.; Pathak, D.; Ghotekar, S. Recent trends in synthesis of 2D MXene-based materials for sustainable environmental applications. *Emergent Materials* **2024**, *7* (1), 35−62.

(22) Kwon, O.; Choi, Y.; Kang, J.; Kim, J. H.; Choi, E.; Woo, Y. C.; Kim, D. W. A comprehensive review of MXene-based water-treatment membranes and technologies: Recent progress and perspectives. *Desalination* **2022**, *522*, No. 115448.

(23) Wang, H.; Peng, R.; Hood, Z. D.; Naguib, M.; Adhikari, S. P.; Wu, Z. Titania Composites with 2 D Transition Metal Carbides as Photocatalysts for Hydrogen Production under Visible-Light Irradiation. *ChemSusChem* **2016**, *9* (12), 1490−1497.

(24) Xi, Q.; Yue, X.; Feng, J.; Liu, J.; Zhang, X.; Zhang, C.; Wang, Y.; Wang, Y.; Lv, Z.; Li, R.; Fan, C. Facile synthesis of 2D Bi4O5Br2/2D thin layer-Ti3C2 for improved visible-light photocatalytic hydrogen evolution. *J. Solid State Chem.* **2020**, *289*, No. 121470.

(25) Park, Y. H.; Murali, G.; Modigunta, J. K. R.; In, I.; In, S.-I. Recent advances in quantum dots for photocatalytic CO2 reduction: a mini-review. *Frontiers in Chemistry* **2021**, *9*, No. 734108.

(26) Parey, V.; Abraham, B. M.; Mir, S. H.; Singh, J. K. High-Throughput Screening of Atomic Defects in MXenes for CO2 Capture, Activation, and Dissociation. *ACS Appl. Mater. Interfaces* **2021**, *13* (30), 35585−35594.

(27) Khan, A. A.; Tahir, M.; Bafaqeer, A. Constructing a Stable 2D Layered Ti3C2MXene Cocatalyst-Assisted TiO2/g-C3N4/Ti3C2 Heterojunction for Tailoring Photocatalytic Bireforming of Methane under Visible Light. *Energy Fuels* **2020**, *34* (8), 9810−9828.

(28) Zeng, Z.; Yan, Y.; Chen, J.; Zan, P.; Tian, Q.; Chen, P. Boosting the Photocatalytic Ability of Cu2O Nanowires for CO2 Conversion by MXene Quantum Dots. *Adv. Funct. Mater.* **2019**, *29* (2), No. 1806500.

(29) Zhang, T.; Debow, S.; Song, F.; Qian, Y.; Creasy, W. R.; DeLacy, B. G.; Rao, Y. Interface Catalysis of Nickel Molybdenum (NiMo) Alloys on Two-Dimensional (2D) MXene for Enhanced Hydrogen Electrochemistry. *J. Phys. Chem. Lett.* **2021**, *12* (46), 11361−11370.

(30) Song, F.; Debow, S.; Zhang, T.; Qian, Y.; Huang-Fu, Z.-C.; Munns, K.; Schmidt, S.; Fisher, H.; Brown, J. B.; Su, Y.; Zander, Z.; DeLacy, B. G.; Mirotznik, M. S.; Opila, R. L.; Rao, Y. Interface Catalysts of Ni3Fe1 Layered Double Hydroxide and Titanium Carbide for High-Performance Water Oxidation in Alkaline and Natural Conditions. *J. Phys. Chem. Lett.* **2023**, *14* (24), 5692−5700.

(31) Peng, Q.; Guo, J.; Zhang, Q.; Xiang, J.; Liu, B.; Zhou, A.; Liu, R.; Tian, Y. Unique Lead Adsorption Behavior of Activated Hydroxyl Group in Two-Dimensional Titanium Carbide. *J. Am. Chem. Soc.* **2014**, *136* (11), 4113−4116.

(32) Shahzad, A.; Rasool, K.; Miran, W.; Nawaz, M.; Jang, J.; Mahmoud, K. A.; Lee, D. S. Two-Dimensional Ti3C2Tx MXene Nanosheets for Efficient Copper Removal from Water. *ACS Sustainable Chem. Eng.* **2017**, *5* (12), 11481−11488.

(33) Zhang, Q.; Li, Y.; Yang, Q.; Chen, H.; Chen, X.; Jiao, T.; Peng, Q. Distinguished Cr(VI) capture with rapid and superior capability using polydopamine microsphere: Behavior and mechanism. *Journal of Hazardous Materials* **2018**, *342*, 732−740.

(34) Ihsanullah, I. Potential of MXenes in Water Desalination: Current Status and Perspectives. *Nano-Micro Letters* **2020**, *12* (1), 72.

(35) Berkani, M.; Smaali, A.; Almomani, F.; Vasseghian, Y. Recent advances in MXene-based nanomaterials for desalination at water interfaces. *Environmental Research* **2022**, *203*, No. 111845.

(36) Zhang, J.; Shao, C.; Lei, Z.; Li, Y.; Bai, H.; Zhang, L.; Ren, G.; Wang, X. Treatment of antibiotics in water by SO3H-modified Ti3C2Mxene photocatalytic collaboration with g-C3N4. *Journal of Materials Science & Technology* **2024**, *194*, 124−137.

(37) Mashtalir, O.; Cook, K. M.; Mochalin, V. N.; Crowe, M.; Barsoum, M. W.; Gogotsi, Y. Dye adsorption and decomposition on two-dimensional titanium carbide in aqueous media. *Journal of Materials Chemistry A* **2014**, *2* (35), 14334−14338.

(38) Wei, Z.; Peigen, Z.; Wubian, T.; Xia, Q.; Yamei, Z.; ZhengMing, S. Alkali treated Ti3C2Tx MXenes and their dye adsorption performance. *Mater. Chem. Phys.* **2018**, *206*, 270−276.

(39) Zhang, L.; Tang, Y.; Khan, A. R.; Hasan, M. M.; Wang, P.; Yan, H.; Yildirim, T.; Torres, J. F.; Neupane, G. P.; Zhang, Y.; Li, Q.; Lu, Y. 2D Materials and Heterostructures at Extreme Pressure. *Advanced Science* **2020**, *7* (24), No. 2002697.

(40) Wang, Y.; Li, M.; Chang, J.-K.; Aurelio, D.; Li, W.; Kim, B. J.; Kim, J. H.; Liscidini, M.; Rogers, J. A.; Omenetto, F. G. Light-activated shape morphing and light-tracking materials using biopolymer-based programmable photonic nanostructures. *Nat. Commun.* **2021**, *12* (1), 1651.

(41) Kumar, N.; Najmaei, S.; Cui, Q.; Ceballos, F.; Ajayan, P. M.; Lou, J.; Zhao, H. Second harmonic microscopy of monolayer MoS${}_{2}$. *Phys. Rev. B* **2013**, *87* (16), No. 161403.

(42) Malard, L. M.; Alencar, T. V.; Barboza, A. P. M.; Mak, K. F.; de Paula, A. M. Observation of intense second harmonic generation from MoS${}_{2}$ atomic crystals. *Phys. Rev. B* **2013**, *87* (20), No. 201401.

(43) Li, Y.; Rao, Y.; Mak, K. F.; You, Y.; Wang, S.; Dean, C. R.; Heinz, T. F. Probing Symmetry Properties of Few-Layer MoS2 and h-BN by Optical Second-Harmonic Generation. *Nano Lett.* **2013**, *13* (7), 3329−3333.

(44) Ribeiro-Soares, J.; Janisch, C.; Liu, Z.; Elías, A. L.; Dresselhaus, M. S.; Terrones, M.; Cançado, L. G.; Jorio, A. Second Harmonic Generation in WSe2. *2D Materials* **2015**, *2* (4), No. 045015.

(45) Zhou, J.; Shi, J.; Zeng, Q.; Chen, Y.; Niu, L.; Liu, F.; Yu, T.; Suenaga, K.; Liu, X.; Lin, J.; Liu, Z. InSe monolayer: synthesis, structure and ultra-high second-harmonic generation. *2D Materials* **2018**, *5* (2), No. 025019.

(46) He, C.; Wu, R.; Zhu, L.; Huang, Y.; Du, W.; Qi, M.; Zhou, Y.; Zhao, Q.; Xu, X. Anisotropic Second-Harmonic Generation Induced by Reduction of In-Plane Symmetry in 2D Materials with Strain Engineering. *J. Phys. Chem. Lett.* **2022**, *13* (1), 352−361.

(47) Hou, C.; Shen, Y.; Wang, Q.; Kawazoe, Y.; Jena, P. Large second harmonic generation in a penta-CdO2 sheet exfoliated from its bulk phase. *Journal of Materials Chemistry A* **2022**, *11* (1), 167−177.

(48) Han, Z.; Han, X.; Wu, S.; Zhang, Q.; Hu, W.; Meng, Y.; Liang, Y.; Hu, J.; Li, L.; Zhang, Q.; Zhang, Y.; Zhao, X.; Geng, D.; Hu, W. Phase and Composition Engineering of Self-Intercalated 2D Metallic Tantalum Sulfide for Second-Harmonic Generation. *ACS Nano* **2024**, *18* (8), 6256−6265.

(49) He, C.; Zhao, Q.; Huang, Y.; Du, W.; Zhu, L.; Zhou, Y.; Zhang, S.; Xu, X. Strain-dependent anisotropic nonlinear optical response in two-dimensional functionalized MXene Sc2CT2 (T = O and OH). *Phys. Chem. Chem. Phys.* **2020**, *22* (37), 21428−21435.

(50) Tan, D.; Jiang, C.; Sun, N.; Huang, J.; Zhang, Z.; Zhang, Q.; Bu, J.; Bi, S.; Guo, Q.; Song, J. Piezoelectricity in monolayer MXene for nanogenerators and piezotronics. *Nano Energy* **2021**, *90*, No. 106528.

(51) Jhon, Y. I.; Jhon, Y. M.; Lee, J. H. Nonlinear optics of MXene in laser technologies. *Journal of Physics: Materials* **2020**, *3* (3), No. 032004.

(52) Jhon, Y. I.; Koo, J.; Anasori, B.; Seo, M.; Lee, J. H.; Gogotsi, Y.; Jhon, Y. M. Metallic MXene Saturable Absorber for Femtosecond Mode-Locked Lasers. *Adv. Mater.* **2017**, *29* (40), No. 1702496.

(53) Jiang, X.; Liu, S.; Liang, W.; Luo, S.; He, Z.; Ge, Y.; Wang, H.; Cao, R.; Zhang, F.; Wen, Q.; Li, J.; Bao, Q.; Fan, D.; Zhang, H. Broadband Nonlinear Photonics in Few-Layer MXene Ti3C2Tx (T = F, O, or OH). *Laser & Photonics Reviews* **2018**, *12* (2), No. 1700229.

(54) Cao, L.; Chu, H.; Pan, H.; Wang, R.; Li, Y.; Zhao, S.; Li, D.; Zhang, H.; Li, D. Nonlinear optical absorption features in few-layered hybrid Ti3C2(OH)2/Ti3C2F2MXene for optical pulse generation in the NIR region. *Opt. Express* **2020**, *28* (21), 31499−31509.

(55) Zhang, T.; Chu, H.; Li, Y.; Zhao, S.; Li, D. Third-order nonlinear properties and reverse absorption behavior in layered Ti3C2MXene in the near infrared region. *Opt. Mater. Express* **2021**, *11* (12), 4051−4057.

(56) Shang, C.; Zhang, Y.; Wang, G.; Sun, J.; Cheng, Y.; Zhang, Y.-B.; Yao, B.; Fu, B.; Li, J. Nonlinear optical properties of MXene and applications in broadband ultrafast photonics. *J. Alloys Compd.* **2022**, *918*, No. 165580.

(57) Volkov, M.; Willinger, E.; Kuznetsov, D. A.; Müller, C. R.; Fedorov, A.; Baum, P. Photo-Switchable Nanoripples in Ti3C2Tx MXene. *ACS Nano* **2021**, *15* (9), 14071−14079.

(58) Li, H.; Chen, S.; Boukhvalov, D. W.; Yu, Z.; Humphrey, M. G.; Huang, Z.; Zhang, C. Switching the Nonlinear Optical Absorption of Titanium Carbide MXene by Modulation of the Surface Terminations. *ACS Nano* **2022**, *16* (1), 394−404.

(59) Debow, S.; Zhang, T.; Liu, X.; Song, F.; Qian, Y.; Han, J.; Maleski, K.; Zander, Z. B.; Creasy, W. R.; Kuhn, D. L.; Gogotsi, Y.; DeLacy, B. G.; Rao, Y. Charge Dynamics in TiO2/MXene Composites. *J. Phys. Chem. C* **2021**, *125* (19), 10473−10482.

(60) Peleg, G.; Lewis, A.; Linial, M.; Loew, L. M. Nonlinear optical measurement of membrane potential around single molecules at selected cellular sites. *Proc. Natl. Acad. Sci. U. S. A.* **1999**, *96* (12), 6700−6704.

(61) Butet, J.; Brevet, P.-F.; Martin, O. J. F. Optical Second Harmonic Generation in Plasmonic Nanostructures: From Fundamental Principles to Advanced Applications. *ACS Nano* **2015**, *9* (11), 10545−10562.

(62) Wang, H.; Zhang, J.; Wu, Y.; Huang, H.; Jiang, Q. Chemically functionalized two-dimensional titanium carbide MXene by in situ grafting-intercalating with diazonium ions to enhance supercapacitive performance. *J. Phys. Chem. Solids* **2018**, *115*, 172−179.

(63) Riazi, H.; Anayee, M.; Hantanasirisakul, K.; Shamsabadi, A. A.; Anasori, B.; Gogotsi, Y.; Soroush, M. Surface Modification of a MXene by an Aminosilane Coupling Agent. *Advanced Materials Interfaces* **2020**, *7* (6), No. 1902008.

(64) Lin, H.; Wang, X.; Yu, L.; Chen, Y.; Shi, J. Two-Dimensional Ultrathin MXene Ceramic Nanosheets for Photothermal Conversion. *Nano Lett.* **2017**, *17* (1), 384−391.

(65) Liu, W.; Wang, L.; Ding, L.; Zhang, C.; Yang, W.; Liu, D.; Hu, W. Boron-Based Polyphosphazene-Functionalized Mxene Nanosheets for Polypropylene Composites with Improved Mechanical Properties and Flame Retardancy Applications. *ACS Applied Nano Materials* **2024**, *7* (2), 2021−2032.

(66) Hao, C.; Li, G.; Wang, G.; Chen, W.; Wang, S. Preparation of acrylic acid modified alkalized MXene adsorbent and study on its dye adsorption performance. *Colloids Surf., A* **2022**, *632*, No. 127730.

(67) Yan, Y.; Han, H.; Dai, Y.; Zhu, H.; Liu, W.; Tang, X.; Gan, W.; Li, H. Nb2CTx MXene Nanosheets for Dye Adsorption. *ACS Applied Nano Materials* **2021**, *4* (11), 11763−11769.

(68) Anayee, M.; Shuck, C. E.; Shekhirev, M.; Goad, A.; Wang, R.; Gogotsi, Y. Kinetics of Ti3AlC2 Etching for Ti3C2Tx MXene Synthesis. *Chem. Mater.* **2022**, *34* (21), 9589−9600.

(69) Thakur, A.; Chandran B.S, N.; Davidson, K.; Bedford, A.; Fang, H.; Im, Y.; Kanduri, V.; Wyatt, B. C.; Nemani, S. K.; Poliukhova, V.; Kumar, R.; Fakhraai, Z.; Anasori, B. Step-by-Step Guide for Synthesis and Delamination of Ti3C2Tx MXene. *Small Methods* **2023**, *7* (8), No. 2300030.

(70) Chen, L.; Wakeel, M.; Haq, T. U.; Chen, C.; Ren, X. Insight into UV-induced simultaneous photocatalytic degradation of Ti3C2Tx MXene and reduction of U(VI). *Journal of Hazardous Materials* **2022**, *430*, No. 128377.

(71) Zhang, Q.; Lai, H.; Fan, R.; Ji, P.; Fu, X.; Li, H. High Concentration of Ti3C2Tx MXene in Organic Solvent. *ACS Nano* **2021**, *15* (3), 5249−5262.

(72) Zhang, K.; Di, M.; Fu, L.; Deng, Y.; Du, Y.; Tang, N. Enhancing the magnetism of 2D carbide MXene Ti3C2Tx by H2 annealing. *Carbon* **2020**, *157*, 90−96.

(73) Luo, Y.; Chen, G.-F.; Ding, L.; Chen, X.; Ding, L.-X.; Wang, H. Efficient Electrocatalytic N2 Fixation with MXene under Ambient Conditions. *Joule* **2019**, *3* (1), 279−289.

(74) Firestein, K. L.; von Treifeldt, J. E.; Kvashnin, D. G.; Fernando, J. F. S.; Zhang, C.; Kvashnin, A. G.; Podryabinkin, E. V.; Shapeev, A. V.; Siriwardena, D. P.; Sorokin, P. B.; Golberg, D. Young's Modulus and Tensile Strength of Ti3C2MXene Nanosheets As Revealed by In

Situ TEM Probing, AFM Nanomechanical Mapping, and Theoretical Calculations. *Nano Lett.* **2020**, *20* (8), 5900−5908.

(75) Qian, Y.; Brown, J. B.; Huang-Fu, Z.-C.; Zhang, T.; Wang, H.; Wang, S.; Dadap, J. I.; Rao, Y. In situ analysis of the bulk and surface chemical compositions of organic aerosol particles. *Communications Chemistry* **2022**, *5* (1), 58.

(76) Wang, H.; Yan, E. C. Y.; Borguet, E.; Eisenthal, K. B. Second harmonic generation from the surface of centrosymmetric particles in bulk solution. *Chem. Phys. Lett.* **1996**, *259* (1), 15−20.

(77) Roke, S.; Gonella, G. Nonlinear Light Scattering and Spectroscopy of Particles and Droplets in Liquids. *Annu. Rev. Phys. Chem.* **2012**, *63*, 353−378.

(78) de Beer, A. G. F.; Roke, S. Obtaining molecular orientation from second harmonic and sum frequency scattering experiments in water: Angular distribution and polarization dependence. *J. Chem. Phys.* **2010**, *132* (23), No. 234702.

(79) Schürer, B.; Wunderlich, S.; Sauerbeck, C.; Peschel, U.; Peukert, W. Probing colloidal interfaces by angle-resolved second harmonic light scattering. *Phys. Rev. B* **2010**, *82* (24), No. 241404.

(80) Wei, X.; Hong, S.-C.; Zhuang, X.; Goto, T.; Shen, Y. R. Nonlinear optical studies of liquid crystal alignment on a rubbed polyvinyl alcohol surface. *Phys. Rev. E* **2000**, *62* (4), 5160−5172.

(81) Ying, G.; Dillon, A. D.; Fafarman, A. T.; Barsoum, M. W. Transparent, conductive solution processed spincast 2D Ti2CTx (MXene) films. *Materials Research Letters* **2017**, *5* (6), 391−398.

(82) Boyd, R. W. Chapter 1 - The Nonlinear Optical Susceptibility. In *Nonlinear Optics*, 3rd ed.; Boyd, R. W., Ed.; Academic Press: 2008; pp 1−67.

(83) Wang, H.; Yan, E. C. Y.; Liu, Y.; Eisenthal, K. B. Energetics and Population of Molecules at Microscopic Liquid and Solid Surfaces. *J. Phys. Chem. B* **1998**, *102* (23), 4446−4450.

(84) Swenson, H.; Stadie, N. P. Langmuir's Theory of Adsorption: A Centennial Review. *Langmuir* **2019**, *35* (16), 5409−5426.

(85) Castro, A.; Bhattacharyya, K.; Eisenthal, K. B. Energetics of adsorption of neutral and charged molecules at the air/water interface by second harmonic generation: Hydrophobic and solvation effects. *J. Chem. Phys.* **1991**, *95* (2), 1310−1315.

(86) Eckenrode, H. M.; Jen, S.-H.; Han, J.; Yeh, A.-G.; Dai, H.-L. Adsorption of a Cationic Dye Molecule on Polystyrene Microspheres in Colloids: Effect of Surface Charge and Composition Probed by Second Harmonic Generation. *J. Phys. Chem. B* **2005**, *109* (10), 4646−4653.